ROYAL SOCIETY
OF CHEMISTRY

PAPER

Check for updates

Construction of a drug-containing microenvironment for *in situ* bone regeneration†

Zhen Wu,[a] Zhou Zhong,[b] Wenchao He,[a] Yanmei Wu,[a] Yuyan Cai,[a] Huilin Yang[c] and Youliang Hong [iD] *[a]

The construction of bone scaffolds to treat bone defects caused by infection is a major challenge because such bone scaffolds need to both prevent infection from recurring and regenerate bone defects. To this end, we constructed bioactive glass (BG)-coated, hierarchical porous tricalcium phosphate (TCP) ceramics as both bone scaffolds and drug delivery devices to treat *S. aureus*-infected bone defects. *In vitro* simulation experiments confirmed that the as-prepared porous ceramics could construct a dynamic microenvironment, in which the concentration of the released antibiotics and calcium ions always changed and an apatite layer could grow on the ceramic surfaces. *In vitro* experiments demonstrated that antibiotic-loaded ceramics possessed good cytocompatibility and the microenvironment established by the antibiotic-loaded ceramics could mediate the osteogenic commitment of mesenchymal stem cells (MSCs), and at the same time, the antibiotic-loaded ceramics presented excellent and relatively-lasting antibacterial activity. *In vivo* experiments demonstrated that the antibiotic-loaded ceramics not only could prevent the *S. aureus*-infected bone defects from recurring, but also could boost the endogenous regeneration of bone.

1. Introduction

It is of clinical significance to tailor biomaterials into porous scaffolds that can create a microenvironment (also called a niche) to mediate *in situ* bone regeneration,[1–6] and thus the exploration of the microenvironmental factors that can stimulate/activate an endogenous regenerative procedure of bones becomes an important topic in the bone tissue engineering field. To this end, some microenvironmental factors that could be administrated by biomaterials, *e.g.*, pH,[7–9] the concentration of calcium/phosphate ions,[9–11] the formation of an apatite layer,[12–15] surface topographies,[16,17] *etc.*, have been demonstrated to be able to mediate the osteogenic commitment of MSCs and *in situ* bone regeneration. In particular, our recent work has demonstrated that a dynamic microenvironment

established by a gypsum-coated TCP scaffold could promote native healing cascades of bone defects.[18]

Still, current experiments mainly focused on exploring the scaffold-constructed microenvironment to regenerate bone defects arising from healthy bone. In actual clinical cases, however, plenty of bone defects arise from specific diseases, *e.g.*, tumours, bone infection, *etc.* To treat disease-caused bone defects, two medical problems need to be tackled: (i) prevent the tumour/infection from recurring, and (ii) regenerate bone defects. Therefore, it is found that the scaffold-created microenvironment not only can mediate bone regeneration, but also can prevent disease recurrence.

Currently, the strategy of local drug administration,[19–22] the construction of local delivery devices using biomaterials (*e.g.*, PMMA, bioactive glass, calcium sulfates, and calcium phosphates),[23] and the loading of antibacterial materials (*e.g.*, graphene oxide nanosheets/polydopamine and polydopamine/silver nanoparticles) onto the scaffolds[24–26] are well developed to treat the disease-caused bone defects. Still, no attention has been paid to the microenvironment formed by the drug-loaded devices. In particular, it is unclear and thus needs to be investigated whether the introduction of drugs into the microenvironment created by scaffolds will affect the endogenous bone regeneration.

Here, our aim is to study the endogenous bone regeneration mediated by a drug-containing microenvironment. To this end, we design triple hierarchical porous bioceramics as bone

[a] *National Engineering Research Centre for Biomaterials; Department of Biomedical Engineering, Sichuan University, Chengdu, 610064, P. R. China.*
E-mail: hyl@scu.edu.cn
[b] *Department of Orthopaedic Surgery, West China Hospital, Sichuan University, Chengdu 610041, P. R. China*
[c] *Department of Orthopaedics, The first Hospital Affiliated to Suzhou University, Suzhou, 215006, P. R. China*
† Electronic supplementary information (ESI) available: The chemical components of the TCP slurry and the BG precursors; detailed information about the primer sequences used for qRT-PCR; the created bone defects and the ceramic implanting experiments; bone infection model and the outcomes of the established bone infection; and the SEM images of the ceramics when soaked in SBF for 36 h. See DOI: https://doi.org/10.1039/d2ma00057a
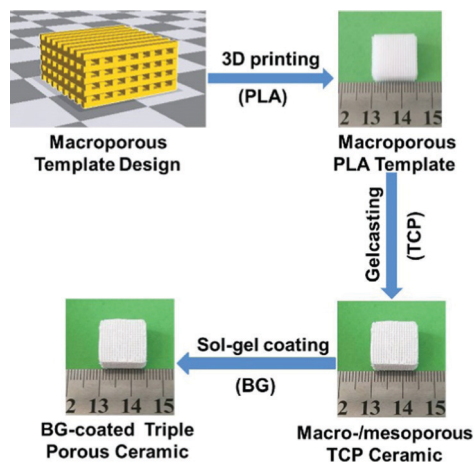
Scheme 1 The illustrative procedure of the preparation of the BG-coated triple hierarchical porous bioceramics.

scaffolds and drug-loaded devices. In detail, we select bioactive materials, TCP and BG, as tailoring objectives, and combine multiple manufacturing techniques, including 3D printing, gelcasting, and nanoporous sol–gel coating techniques, to construct triple hierarchical porous bioceramics. The manufacturing process for the desired products is illustrated in Scheme 1. Bioceramics were designed into hierarchical porous structures because studies of Hollister[27] and our group[18] have demonstrated that the bone scaffolds with right porous structures play important roles in constructing a microenvironment of bone growth, especially, abundant nanopores (*e.g.*, <50 nm) distributed within scaffolds can both improve the bioactivity of scaffolds and serve as delivery vehicles for drugs.[10–14] TCP is selected because it is similar to the mineral components of hard tissues and has now become one of the optimal bone filling materials in clinical practice. Also, BG has been widely applied as a bone repair material.[28] More importantly, BG can release metal ions (*e.g.*, Ca^{2+}) rapidly and possibly establishes a weak alkaline microenvironment to affect bone regeneration.[29,30] In addition, BG can be processed into a thin membrane with abundant nanopores, which can load drugs.[31–33] Finally, gentamicin sulphate (GS), a kind of broad-spectrum antibiotic, is used in this work to construct a drug-containing microenvironment.

2. Experimental

2.1. Materials

Absolute alcohol, dichloromethane (DCM), polymethacrylate (PMA), acrylamide (AM), hydrochloric acid (HCl), *N*,*N*,*N'*,*N'*-tetramethylethylenediamine (TMED), ammonium persulfate (APS), *N*,*N'*-methylene bisacrylamide (MBAM), tetraethyl orthosilicate (TEOS), Ca(NO₃)₂·4H₂O, and non-ionic surfactant P123 (poly(ethylene oxide)₂₀–poly(propylene oxide)₇₀–poly(ethyl oxide)₂₀ all are of analytical reagent (AR) grade and were purchased from Chengdu Kelong Reagent Co., China. Hydroxy-propyl methylcellulose (HPMC) was purchased from Shang-dong Weifang Lite Composite Materials Co., China. TCP

powders were prepared using a co-precipitation method and were sintered at 700 °C for 2 h.[34] GS is purchased from Sichuan Changzheng Pharmaceutical Co. Water used in all experiments has been purified using a reverse osmosis (RO) water system.

2.2. Preparation of hierarchical porous bioceramics

At first, porous TCP bioceramics were prepared in light of our previous methods.[18] In brief, a fused deposition modelling (FDM) 3D printer (JGAURORA, Shenzhen Aurora Technology Co.) was used to print porous PLA scaffolds according to the designed STL format files as the ceramic templates. According to different experimental requirements, scaffold prototypes (pore: 0.4 mm and rod: 0.4 mm) with various shapes (*e.g.*, cylinders and cubes) were designed using the 3D design software Solidworks. Then, the TCP slurry was prepared according to the protocol (Table S1, ESI†) and was cast into porous PLA templates. After the TCP slurry solidified, porous PLA templates were removed and the remaining porous TCP green bodies were sintered at 1100 °C in air for 4 h to obtain bimodal porous TCP ceramics. Finally, the surface coating of BG to TCP ceramics was performed. In detail, BG precursors were prepared in light of the protocol (Table S2, ESI†) and then the as-prepared TCP ceramics were soaked under vacuum into BG precursors. 10 min later, the TCP ceramics were removed from the BG precursors and dried in air and then were sintered at 700 °C for 10 h to remove the organic components.

2.3. Drug loading and release

The BG-coated TCP (BG-TCP) ceramics were soaked into GS aqueous solution (the GS concentration was 40 mg ml⁻¹) in a vacuum. After 10 min, the ceramics were removed and dried in air. The GS loading amount in ceramics was analysed by measuring the GS concentration before and after porous ceramic soaking through fluorescence spectroscopy using an o-phthaldi-aldehyde (OPA) reagent. It reacts with the amino groups of GS to produce fluorescence that was determined (excitation wavelength = 340 nm and emission wavelength = 441 nm) by fluorescence spectroscopy and then by using the following formula, $L_G\% = [(C_b/V_b - C_a/V_a)/W_c] \times 100$, where C_b and C_a are the GS concentration before and after porous ceramic soaking, V_b and V_a are the volume of the GS solution before and after porous ceramic soaking, and W_c is the weight of porous ceramics.

The GS release dynamics were analysed by soaking six parallel GS-loaded ceramics (160 mg) into RO water (20 ml)/simulated body fluid (SBF) (20 ml). The soaking liquid was incubated at 37 °C in a thermostat shaker. At appropriate intervals part of the incubated liquid (10 ml) was removed for monitoring by fluorescence spectroscopy as described above, and at the same time, the soaking liquid was replenished with 10 ml fresh liquid. The quantity of GS released was calculated to determine the drug release kinetics of GS.

2.4. Ion release analysis and pH measurements

The as-prepared ceramics (20 mg) were soaked in 37 °C SBF (20 ml). At appropriate intervals part of the incubated SBF (10 ml)

was removed for pH and ion concentration analysis and the same volume of fresh SBF was replenished. The calcium/phosphate ion concentration in the soaked SBF was measured by using a calcium colorimetric assay kit (Beyotime S10635) and a tissue inorganic phosphorus content assay kit (Solarbio BC2845). The silica concentration was measured using inductively coupled plasma atomic emission spectrometry (ICP-AES) (PerkinElmer Optima, 7000DV), and before analysis, the organic components in the soaked liquid were removed by the heating and redissolving method (*i.e.*, the soaked SBF was heated at 80 °C and sintered at 800 °C for 4 h, and the formed sediment was dissolved in 5 ml of 1 M HCl).

2.5. The growth of the apatite layer on the ceramic surfaces

Porous TCP, BG-TCP, and GS-loaded BG-TCP (GS/BG-TCP) ceramics were soaked in a simulated body fluid (SBF) over time to grow a bone-like nanoapatite layer. The process of nanoapatite layer growth was observed using a Scanning Electron Microscope (SEM) (Hitachi S-4800).

2.6. Physicochemical characterization

2.6.1. SEM and energy-dispersive X-ray spectroscopy (EDX). At first, the samples were coated with a thin layer of gold using a gold sputter (E-1010, Hitachi) (the coating time was 120 s). Then the samples were observed by SEM, and the element distribution of the samples was analysed using an EDX instrument (Oxford IE250).

2.6.2. Transmission electron microscopy (TEM). The BG coated on the surfaces of the TCP ceramics was observed using a TEM (Tecnai G2 F20 S-TWIN, FEI). Before measurement, the BG-TCP ceramics were ground into fine powders which were dispersed in absolute ethanol, and the suspension droplets were dropped onto the carbon film coated copper grid (400 mesh) for TEM observation.

2.6.3. Mechanical testing. The compressive strength of the porous ceramics was tested using a 20 kN loading capacity universal testing machine (AG-IC, Shimadz). In detail, the as-prepared ceramics were tailored into cubes with size 12 × 12 × 6 mm and were fixed to the universal testing machine. The ceramics were measured using a speed of 3.0 mm min^{-1} until cracking.

2.6.4. Porosity testing. A mercury intrusion porosimeter (MIP, micromeritics Auto Pore IV9500) was used to measure the cumulative pore volume, average pore diameter, pore diameter distribution, and porosity of ceramics. At the same time, N$_2$ sorption experiments were conducted using a micromeritics Gemini instrument. The ceramics were degassed at 100 °C *in vacuo* for 12 h prior to investigation.

2.7 *In vitro* biological functions of porous ceramics

2.7.1. Isolation and culture of BM-MSCs. Neonatal Sprague-Dawley (SD) rats (3–5 days) were purchased from the Chengdu Dossy Experimental animal Co. Animal experiments were approved by the Sichuan University Committee on Animal Care and Use (Grant No. KS2020392). BM-MSCs were harvested from the femoral marrow cavity of the neonatal SD rats that had

been killed by cervical decortication. The harvested BM-MSCs were passaged and the passaged 2 BM-MSCs (2×10^4) were seeded on the ceramic surfaces. The cell-seeded ceramics were cultured at 37 °C in a humid 5% CO$_2$-containing atmosphere. Culture media were changed once every two days. The culture medium was a mixed liquid consisting of α-MEM (89 vol%, Hyclone), fetal bovine serum (FBS; 10 vol%, Gibco), and peni-cillin–streptomycin (1 vol%, Hyclone). Before cell culture, the ceramics were sterilized *via* ultraviolet irradiation for 45 min and were placed into 48-well plates (Corning, USA) and seeded with cells per well in 4 ml of medium.

2.7.2. SEM observation of the cultured cells. The BM-MSCs cultured on the sample surfaces over time were rinsed thrice with sterile phosphate buffered saline (PBS, Hyclone) and fixed by 2.5% glutaraldehyde for 2 h, and then washed twice with PBS. The fixed cells were dehydrated in a graded ethanol series from 30, 50, 70, 80, 90, and 100% ethanol at 20 min interval. The samples were then placed into a critical point drying apparatus (Hitachi) to remove ethanol (27 °C). The samples containing cells were coated with gold using a sputter coater (15 mA, 120 s, Hitachi) and the adhered cells were observed using the SEM at 5.0 kV.

2.7.3. Cell viability and proliferation assessment. Cell viability and proliferation were tested by a quantitative CCK8 assay. In detail, the BM-MSCs cultured with samples for 1, 3, and 5 days were washed thrice with SBF and stained with a mixed reagent consisting of 90% α-MEM and 10% CCK 8 (Dongren Chem. S&T Co, China) (500 μL per well), and the cells were incubated at 37 °C for 2 h in the dark. The cell-incubated CCK8 reagent was then measured at 450 nm using a microplate reader (Bio-Rad model 550, USA). The relative cell viability was calculated according to the formula V_{cell} (%) = $(OD_S - OD_B)/(OD_C - OD_B) \times 100$, where V_{cell} denotes the cell viability, OD_S the absorbance value of the sample, OD_B the absorbance value of the blank, and OD_C the absorbance value of a control (*i.e.*, the cells were always incubated with a common cell medium). The samples were tested in triplicate.

2.7.4. Dead–live staining. The BM-MSCs cultured with samples for 1, 3, and 5 days were rinsed with PBS and stained by fluorescein diacetate (FDA, 1 μg ml^{-1}) for live cells (green) and propidium iodide (PI, 5 μg ml^{-1}) for dead cells (red) (FDA and PI were purchased from Yeasen Biotechnol. Co., Shanghai). The stained cells were observed using a confocal laser scanning microscope (CLSM, Olympus IX 95).

2.7.5. Phalloidin staining. The cytoskeleton of the cells cultured on the ceramic surfaces for 1 day was stained according to the manufacturer's protocol. In detail, the cells were rinsed thrice using PBS and fixed using formaldehyde (4%) for 10 min and then washed thrice with PBS again. Then, the cells were dehydrated with acetone and permeabilized in 0.1% Triton X-100 containing PBS for 5 min, and then washed thrice with PBS. Finally, the cells were stained with rhodamine–phalloidin conjugate solution (10 μg ml^{-1}, Yeasen Biotechnol. Co.) for 40 minutes at 37 °C, and the cells were washed thrice with PBS to remove unbound phalloidin conjugates. For nuclear visualization, a small drop of DAPI solution (5μg ml^{-1}, Yeasen

Biotechnol. Co.) was added. The samples were observed by CLSM.

2.7.6. Alkaline phosphatase (ALP) staining. The BM-MSCs cultured with samples for 4 days were washed thrice with PBS and fixed with formaldehyde (4%) for 15 min and then washed thrice with PBS again. The fixed BM-MSCs were stained with drops of 500 μl 5-bromo-4-chloro-3-indolyl-phosphate/Nitro-Blue-Tetrazolium Alkaline Phosphatase Color Development Kit solution (Beyotime, China) and then incubated for 30 min, and finally washed thrice with PBS. The cells were observed using a stereo microscope (Zeiss, SteREO Discovery. V20).

2.7.7. Osteocalcin (OCN) immunofluorescence staining. The cells cultured with slices for 14 days were rinsed thrice with PBS and fixed with paraformaldehyde (4%) for 15 min and then washed thrice with PBS again. The fixed BM-MSCs were permeabilized in 0.5% Triton X-100 containing PBS for 20 min, and then washed thrice with PBS. Next, the cells were blocked using 10% Lowenthal serum (diluted by 1% BSA) and incubated for 30 min at room temperature, and then primary antibodies (anti-OCN, Abclonal, A6205) were added and incubated overnight at 4 °C. After the cells were washed thrice with PBS, a biotinylated secondary antibody (Abclonal, AS011) was added and incubated for 1 h at room temperature. The cells were washed trice with PBS and stained by DAPI (5 μg ml^{-1}). The stained cells were observed using a CLSM.

2.7.8. Quantitative real-time PCR. The cells cultured on the ceramic surfaces for 4, 7, and 14 days were washed thrice with PBS, and then the total RNA was isolated using 300 μl Trizol reagent in light of the manufacturer's protocol and collected by ethanol precipitation. The collected RNA was dissolved in 30 μl DEPD water. RNA was reverse transcribed into complementary DNA (cDNA) using a PrimeScript™ RT reagent Kit (Takara). In light of the qPCR Tip Green qPCR SuperMix reagent Kit (TransGen Biotech., China), equal volumes of cDNA were used to program qPCR reactions specific for some osteogenesis-related mRNA encoding, involving RUNX-2, osteopontin (OPN), and OCN. Forward and reverse primers for the above genes were designed and are listed in Table S3 (ESI†). Reactions were performed using a CFX96 real time PCR system (Bio-Rad, USA). The relative mRNA abundance was calculated using the $2^{-\Delta\Delta Ct}$ method and reported as fold induction. GAPDH abundance was used for normalization. The results were normalized by live cell numbers.

2.8. Antibacterial activity assessment of porous ceramics

To assess the antibacterial activity, Gram-positive bacteria *Staphylococcus aureus* (*S. aureus*, ATCC 29213) and Gram-negative bacteria *Escherichia coli* (*E. coli*, ATCC 25922) were used, and the experiments were conducted in an ultraclean table. To determine the antibacterial activity of the ceramics, the methods of both bacterial suspension and disk diffusion (*i.e.*, inhibition zone) were used, and at the same time, a method of sample transfer was created here, *i.e.*, a sample was incubated in turn for 24 h in the fresh bacterial suspensions/disks.

In the bacterial suspension culture, different porous ceramics with three parallel samples were placed into 24-well culture plates, and an LB liquid medium was used as a control. The bacterial liquid (10^6 CFU mL^{-1}), which had been grown in a tryptic soy broth (TSB, BD) overnight in an incubator at 37 °C, was dropped into the wells (200 μL per well). After 24 h of incubation, the porous ceramics were transferred repeatedly into fresh bacterial suspensions to incubate for another 24 h, and the OD value of the cultured bacterial liquid was detected at 600 nm using a microplate reader. The antibacterial rate of the samples was calculated using the formula $A = (OD_C - OD_S)/(OD_C - OD_B) \times 100\%$, where A denotes the antibacterial rate, OD_S is the absorption value of the bacterial liquid with samples, OD_B is the absorption value of the LB medium, and OD_C is the absorption value of the antibacterial liquid without samples.

In the disk diffusion method, the bacterial suspension (100 μL, 10^6 CFU mL^{-1}) was evenly coated on a solid medium, and then ceramics were placed on the solid medium. After being incubated for 24 h at 37 °C, the culture dish with ceramics was observed, and the porous ceramics were transferred repeatedly into fresh bacterium-containing solid medium to incubate for another 24 h.

2.9. *In vivo* biological functions of hierarchical porous ceramics

2.9.1. *In vivo* ceramic implanting. Adult male New Zealand rabbits with weights of 2.5–2.8 kg were purchased from the Experimental Animal Centre of West China College of Pharmacy, Sichuan University, and were adaptively fed for 7 days before surgery. The *in vivo* experiments were conducted strictly in light of state regulations and laws and the Standing Committee on Ethics in China on the use and care of laboratory animals. At the same time, these experiments were done with the guidelines established by the Institute for Experimental Animals of Sichuan University and approved by the Sichuan University Committee on Animal Care and Use (Grant No. KS2020392).

9 adult male New Zealand rabbits were anesthetized by intravenous injection of 1.5 wt% pentobarbital sodium (2 mg kg^{-1}) and the operations were performed under sterile conditions. Then the femoral bone defects (5 mm) were established using an electric drill. The rabbits were evenly divided into 3 groups. Group 1: two porous TCP ceramics were implanted into the marrow cavity and bone defects respectively; Group 2: two BG-TCP porous ceramics were implanted into the marrow cavity and bone defects respectively (Fig. S1, ESI†); and Group 3: the GS/BG-TCP porous ceramics were implanted into bone defects. The sizes of all porous ceramics were the same ($\varnothing$: 5 mm, high: 5 mm). After the ceramics were implanted, the muscle and skin were sealed. GS was injected daily after operation (800 000 U kg^{-1}) for 3 consecutive days. The rabbits with implanted ceramics were sacrificed at 6 weeks. The harvested specimens were fixed with 10% formalin for further histological analysis.

2.9.2. White blood cell (WBC) count. The rabbits implanted with ceramics in the femoral bone defects (5 mm)/marrow cavities for 0, 3 and 6 weeks were investigated. In detail, 2 ml blood was collected from the external ear vein of rabbits using a disposable vacuum tube, and then the WBC

count was carried out *via* a protocol shown as follows. At first, 0.38 ml WBC dilution (PH1066, PHYGENE) was dropped into an Eppendorf tube. Then, 20 μl blood was injected slowly into the bottom of leukocyte dilution and then mixed immediately. After changing into chocolate-brown (red cells had been destroyed completely), the blood-containing WBC dilution (10 ml) was dropped on the counting plate. The WBC count was carried out using an inverted microscope (Leica, DM1000) once the white cells had deposited.

2.9.3. Establishment of the bone infection model. 6 adult male rabbits were weighed and then anesthetized by intravenous injection of 1.5 wt% pentobarbital sodium (2 mg kg^{-1}). After the rabbits had been in a complete coma, the femoral bone defects (5 mm) were established using an electric drill, and then the *S. aureus* suspension (100 μL, 10^8 CFU mL^{-1}) was injected into the bone marrow cavity from the defects. Once the *S. aureus* suspension was injected, the bone defects were sealed using an alginate hydrogel (Fig. S2, ESI†). All the operations were performed under sterile conditions. The *S. aureus*-infected rabbits were fed without antibiotic injection.

2.9.4. Implantation of ceramics into the infected bone defects. 7 days later, the rabbits were anesthetized again. The wounds were opened and marrow was harvested for *in vitro* culture for 24 h to assess whether the bones had been infected (Fig. S3, ESI†). Then the external surface and marrow cavity of the bone were flushed with sterile saline. Finally, the BG-TCP or GS/BG-TCP ceramics (∅: 5 mm, high: 5 mm) were implanted into the bone marrow cavity and bone defects. After the ceramics were implanted, muscle and skin were sealed. The rabbits were fed continuously without antibiotic injection. The ceramic-implanted rabbits were sacrificed at 6 weeks, and specimens were harvested and soaked into 50 mL PBS. After the specimens were soaked with PBS, a little periosteum and marrow were harvested from the specimens and cultured in solid medium at 37 °C for 24 h to observe the growth of bacterial colonies. The specimens were then fixed with 10% formalin for further histological analyses.

2.9.5. Histological analysis. The harvested specimens were sliced into histological sections (thickness: 10–20 μm) by a hard tissue slicing method. The histological sections were fixed with 4% paraformaldehyde at first, then dehydrated in a series of alcohol solutions (70, 80, 90, 95, and 100%), and finally embedded in methylmethacrylate resin. The treated histological sections were stained with toluidine blue (TB) and observed using a stereo and inverted (Leica, DM1000) microscope. The harvested images were analysed statistically using Image J software (v1.8.0).

2.10. Statistical analysis

All data are reported in this work as mean ± standard deviations (s.d.). All data were analyzed using an unpaired Student *t*-test. Confidence levels of >95% (*$p < 0.05$) were considered to be statistically significant.

3. Results and discussion

3.1. Preparation of hierarchical porous BG-TCP bioceramics

To prepare hierarchical porous BG-TCP bioceramics, two processing steps were carried out: porous β-TCP bioceramics were prepared at first, and then the as-prepared TCP bioceramics were coated by BG. In our previous work, we have demonstrated that porous TCP bioceramics with regular macropores could be well prepared by combining the 3D printing and gelcasting
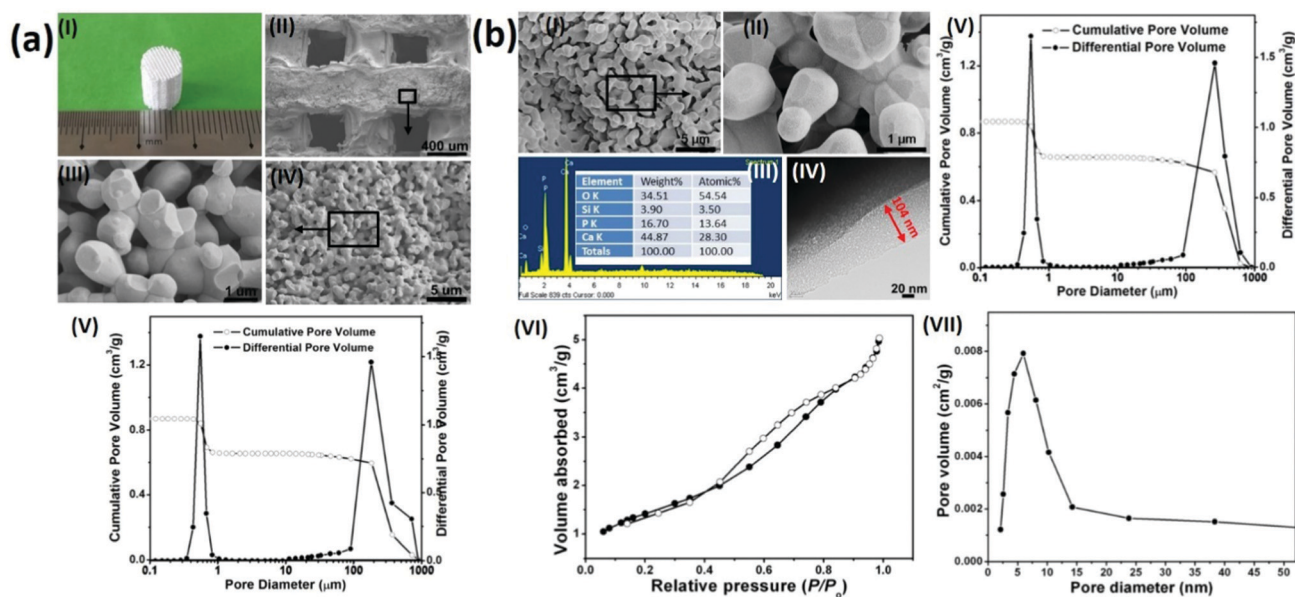

Fig. 1 Preparation of hierarchical porous BG-TCP bioceramics. (a) Preparation of porous TCP bioceramics. (I) Photography, (II–IV) low-, middle- and highly-magnified SEM images, and (V) pore size distribution measured from MIP. (b) The surface coating of BG on porous BG-TCP bioceramics. (I and II) Middle- and highly-magnified SEM images, (III) EDX, (IV) TEM image, (V) MIP, (VI) N2 adsorption–desorption, and (VII) BJH pore size distribution.

techniques.[21] Herein, such a strategy was continuously used to prepare porous TCP bioceramics. Fig. 1a(I) shows a prepared cylindrical porous β-TCP ceramic. SEM images and MIP measurements (Fig. 1a(II–V) and Table 1) show that the as-prepared TCP ceramic was composed of regular macropores (266 μm) and abundant micropores (average diameter: 0.7 μm), and the macroporous and microporous volumes of ceramics were 1.5 and 1.6 cm^3 g^{-1}, respectively. The compressive strength of the TCP bioceramics measured was 2.78 MPa (Table 1).

Subsequently, a sol–gel BG coating onto porous TCP bioceramics was performed to achieve BG-coated TCP ceramics, as shown in Fig. 1(b). SEM images (Fig. 1b(I and II)) show that a thin amorphous layer covered the TCP grain surfaces, and no cracks were displayed in the coating layer. The EDX result (Fig. 1b(III)) shows that besides elements Ca, P, and O, Si was also expressed, demonstrating that the coated amorphous layer was BG. In addition, no element C was present in the EDX curve, demonstrating that no residual organic component remained in the BG matrix. The TEM image (Fig. 1b(IV)) shows that the thickness of the coated BG was ∼104 nm with abundant nanopores (∼6 nm), and the formed nanopores were worm-like and were distributed disorderly in the BG matrix. The MIP result (Fig. 1b(V) and Table 1) shows that the diameter (265 μm) and pore volume (1.5 cm^3 g^{-1}) of the macropores of the ceramic did not change in essence, but both the diameter (0.45 μm) and pore volume (1.2 cm^3 g^{-1}) of the micropores of the ceramic decreased significantly in comparison with those of the TCP bioceramics without the BG coating (macroporous diameter/volume: 266 μm/1.5 cm^3 g^{-1}; microporous diameter/volume: 0.55 μm/1.6 cm^3 g^{-1}, see cm^3 g^{-1} that the porosity of the BG-TCP ceramics also dropped to 69.5%). Still, Table 1 shows that the compressive strength of the BG-TCP bioceramics (3.26 MPa) increased significantly.

The N$_2$ adsorption–desorption isotherm (Fig. 1(VI)) indicates that the isotherm of the as-prepared samples was type IV, and its corresponding Barrett–Joyner–Halenda (BJH) pore size distribution (Fig. 1b(VII)) shows that the average diameter of the nanopores was 6.5 nm, almost in agreement with the TEM observation. The above results well demonstrated that a layer of BG with abundant nanopores (6.5 nm) was coated on the TCP grain surfaces, and the used sol concentration here was suitable for the BG coating.

3.2. *In vitro* microenvironments established by the drug-loaded bioceramics

To understand the osteogenic activity of the GS-loaded bioceramics, especially, to understand the ability of the GS-loaded bioceramics in mediating endogenous bone regeneration, it is essential to evaluate the microenvironment established by the GS-loaded bioceramics. To this end, the experiments of the GS loading and the ceramic soaking (in 37 °C SBF) were carried out at first. The experiments demonstrated that 7.25 wt% GS (the GS/ceramic weight ratio) could be loaded into porous BG-TCP bioceramics. Then, the release dynamics of GS, calcium ions, phosphate ions and silica, pH of the soaked SBF, and the growth of the apatite layer on the ceramic surfaces were investigated in detail.

Fig. 2(a) shows the *in vitro* release profile of GS from the BG-TCP ceramics in SBF. At the initial stage (within 40 h), the average GS release curve shows that the burst release of GS occurred at first, and then (40 h later) the GS release rate decreased. After ∼132 h, the GS release almost ceased from the ceramics. At the releasing peak value (∼ at 40 h), the GS amount in the SBF became 50%. The cumulative release of GS shows that the amount of GS released was *ca* 83.5% when the release of GS from the ceramics ceased (at 160 h), suggesting that 16.5% GS remained in the ceramics. For comparison, Fig. 2(a) shows that the release of GS was faster in water than in SBF. In particular, at the initial stage, the burst release of GS in water was sharper than that in SBF, and after 12 h, the amount of GS released became ∼60%. 100 h later, all GS almost released from the ceramics. The above results suggest that the mineralization reaction of ceramics occurred in SBF, thus impeding the release of GS.

Then, the pH of the soaked SBF was tested. Fig. 2(b) shows that the pH value of the SBF containing the GS/BG-TCP was almost that of weak acid (pH: 6.8). To understand the formation of a weak acid environment, the BG, GS/BG, TCP and BG-TCP ceramics were soaked in SBF respectively. Fig. 2(b) shows that the BG and GS/BG ceramic soaking caused the pH of SBF to increase, but the TCP and BG-TCP ceramic soaking led to a pH decrease of SBF. The above results showed that BG is a kind of alkaline ceramic but TCP is an acidic one,[18,26,27] and in the BG-TCP ceramics, although a layer of BG was coated on the TCP surfaces, TCP predominated in controlling the pH of the ceramics. In the GS-loaded ceramics, because GS was an acid antibiotic (pH: 6), it deceased the pH of the ceramics. Then, the pH of the soaked SBF was tested. Fig. 2(b) shows that the pH value of the SBF containing the GS/BG-TCP was almost that of weak acid (pH: 6.8). To understand the formation of a weak acid environment, the BG, GS/BG, TCP and BG-TCP ceramics were soaked in SBF respectively. Fig. 2(b) shows that the BG and GS/BG ceramic soaking caused the pH of SBF to increase, but the TCP and BG-TCP ceramic soaking led to the pH decrease of SBF. The above results showed that BG is a kind of alkaline ceramic but TCP is an acidic one,[18,26,27] and in the BG-TCP ceramics, although a layer of BG was coated on the TCP surfaces, TCP predominated in controlling the pH of the ceramics. In the GS-loaded ceramics, because GS is an acid antibiotic (pH: 6), it deceased the pH of the ceramics.

Thirdly, the release dynamics of calcium/phosphate ions and silica were analysed. Fig. 2(c) shows that the concentration of Ca^{2+} increased at first, and then decreased, and at the initial stage, the Ca^{2+} concentration was higher than 2.5 mM (the Ca^{2+}

Table 1 Parameters of porous TCP and BG-TCP ceramics

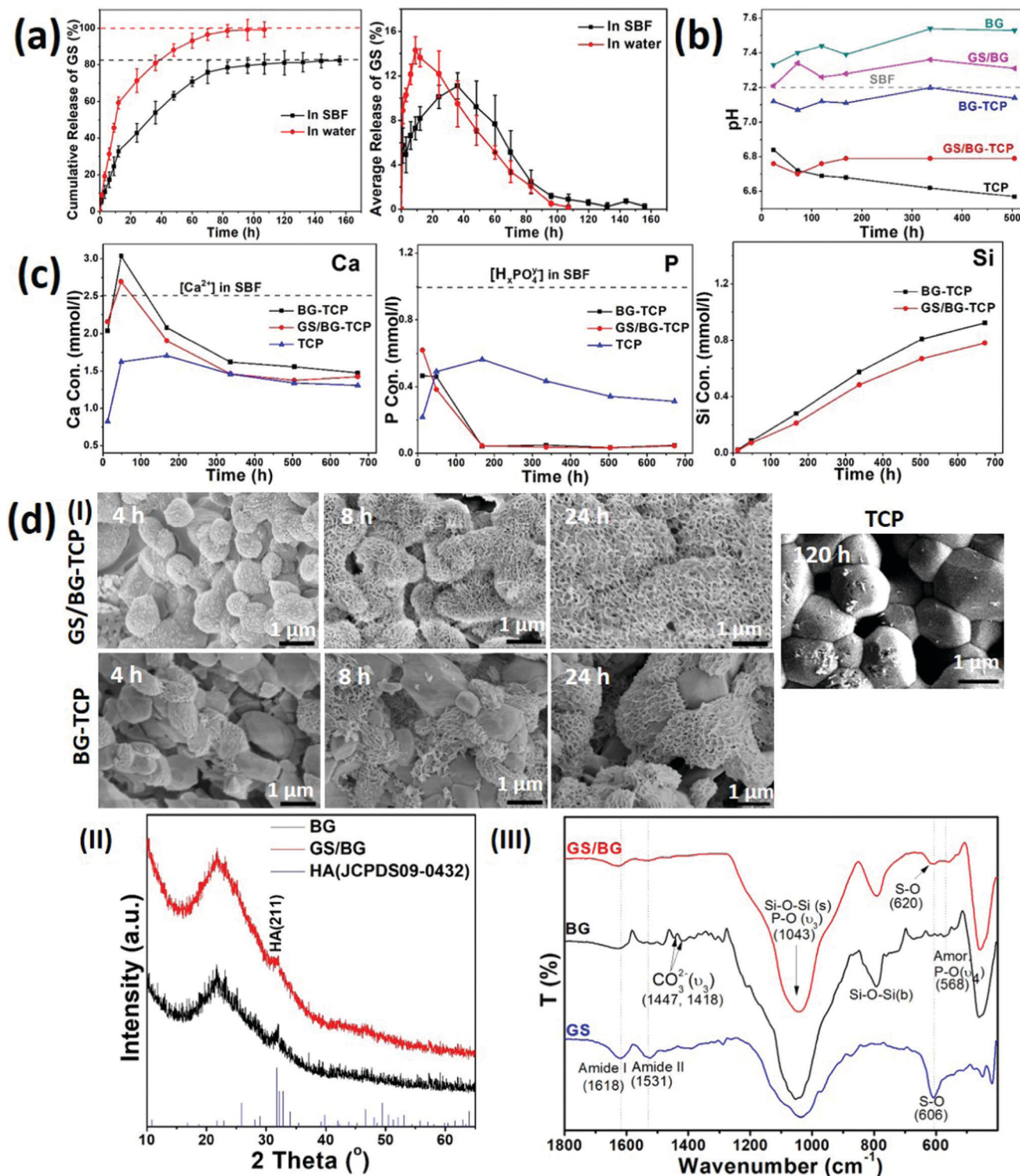|	TCP ceramics	BG-TCP ceramics
Macropore diameter (μm)/volume (cm^3 g^{-1})	266/1.5	265/1.5
Micropore diameter (μm)/volume (cm^3 g^{-1})	0.55/1.6	0.45/1.2
Nanopore diameter (nm)	—	6.5
Compressive strength (MPa)	2.78	3.26

Fig. 2 *In vitro* analysis of the microenvironments constructed by the GS-loaded BG-TCP ceramics in SBF. (a) Cumulative and average release of GS from the BG-TCP ceramics in SBF. Also, the release of GS in water was analysed as a control. (b) The pH value of SBF soaking different samples. (c) The Ca/P/Si release profile from the BG-TCP ceramics with/without GS loading. (d) Surface biomineralization: (I) SEM images of the BG-TCP ceramics with and without GS loading soaked in SBF for 4, 8, and 24 h. For comparison, pure TCP ceramics were soaked in SBF for 120 h. (II) XRD pattern of the BG-TCP ceramics with and without GS loading soaked in SBF for 72 h. (III) FTIR of GS, the SBF soaked BG (soaked in SBF for 72 h), and the SBF soaked GS/BG (72 h).

concentration in SBF was 2.5 mM). The Ca^{2+} concentration higher than that in SBF at the initial stage was significant because Olszak *et al.* have reported that high $[Ca^{2+}]_o$ can recruit immunocytes and MSCs.[35] In contrast, the concentration of phosphate ions was always far lower than 1.0 mM. In comparison with the calcium/phosphate ions, the concentration of
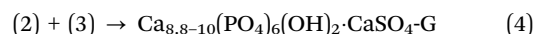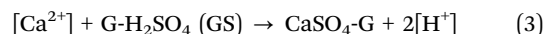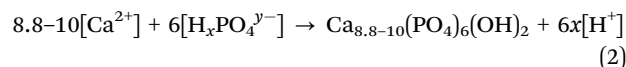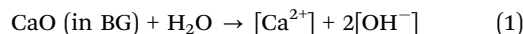
silica increased continuously during the entire release process. The decrease of $[Ca^{2+}]$ and $[H_xPO_4{}^{y-}]$ in SBF could be attributed to the formation of a nano-apatite layer as will be demonstrated afterwards. For comparison, the BG-TCP ceramics without drug loading had a slightly higher $[Ca^{2+}]$ and silica release. The above results suggested that the existence of GS would affect the release of inorganic components.

Finally, the surface mineralization of the GS/BG-TCP ceramics was analysed. Fig. 2d(I) shows that after 4 h SBF immersion, some small nanocrystals homogeneously grew on all grain surfaces. After 8 h soaking, a large amount of nanoplates instead of small nanocrystals covered on all grain surfaces, and 24 h later, more nanoplates formed and the grain profiles could not be observed. In the BG-TCP ceramics without GS loading, however, some nanoplates randomly grew on a few BG-TCP grain surfaces after 4 h SBF immersion, and with the increase of soaking time, more and more apatite nanoplates formed on the surfaces of more BG-TCP grains. Still, the amount of grown nanocrystals was obviously lower than that in the GS-loaded ceramics. For comparison, the pure TCP ceramics were also measured. Fig. 2d(I) shows that only a small number of needle-like nanocrystals formed and deposited on the TCP grain surfaces after 120 h SBF soaking. Such results further confirmed the bioactivity of BG, i.e., the formation of the apatite nanoplates on the ceramic surface was induced by BG. The above results suggested that GS could obviously promote the growth of apatite nanoplates.

To understand the growth of the apatite nanoplates, BG and GS loaded BG (GS/BG) ceramics were prepared and were soaked in SBF for 72 h. The XRD patterns ((Fig. 2d(II)) show that the grown apatite nanoplates in both samples had a low crystal degree. Still, both apatite plates were the hydroxyapatite (HA) phase (JCPDS 09-0432). The FTIR results (Fig. 2d(III)) show that in the GS/BG ceramics, the peaks of amide I/II groups (at 1629/ 1531 cm^{-1}) and P–O groups (the $\upsilon 4$ modes of amorphous phosphate adsorption at 568 cm^{-1} and the $\upsilon 3$ modes of P–O at 1043 cm^{-1})[36] were expressed. Furthermore, the peak at 606 cm^{-1}, assigned to the S–O groups of GS, shifted to 620 cm^{-1}, suggesting that sulfate groups bonded with Ca. The above results demonstrated that the formed nanoplates were the low crystal GS-containing HA, and the existence of GS would take part in the mineralization reaction, thus suggesting that GS could promote the growth of nanoplates and affect the release of GS (Fig. 2a). In the BG ceramics, besides the peaks of the P–O groups, the peaks of the carbonate groups (at 1447 and 1418 cm^{-1}) were present, indicating that the grown nanoplates were low crystal carbonated HA. Such a result suggested that the existence of GS would inhibit the carbonate groups to take part in the mineralization reaction.

Taken together, the above results showed that the GS-loaded BG-TCP ceramics established a dynamic microenvironment, in which the pH and the concentrations of calcium ions, phosphate ions, GS, and silica in SBF always changed. These changes mainly resulted from the release of calcium ions, phosphate ions, GS, and silica and the growth of apatite nanoplates on the ceramic surfaces. At the same time, some

chemical reactions possibly occurred during the release of ions and the growth of nanoplates.

$$CaO \text{ (in BG)} + H_2O \rightarrow [Ca^{2+}] + 2[OH^-] \qquad (1)$$

$$8.8\text{--}10[Ca^{2+}] + 6[H_xPO_4{}^{y-}] \rightarrow Ca_{8.8\text{--}10}(PO_4)_6(OH)_2 + 6x[H^+] \qquad (2)$$

$$[Ca^{2+}] + G\text{-}H_2SO_4 \text{ (GS)} \rightarrow CaSO_4\text{-}G + 2[H^+] \qquad (3)$$

$$(2) + (3) \rightarrow Ca_{8.8\text{--}10}(PO_4)_6(OH)_2 \cdot CaSO_4\text{-}G \qquad (4)$$

When the GS-loaded ceramics were soaked into SBF, CaO within BG surely hydrolyse to release $[Ca^{2+}]$ and increase the pH of SBF (chemical reaction formula (1)). At the same time, $[Ca^{2+}]$ and $[PO_4{}^{3-}]$ released from the TCP ceramics (although the TCP ceramic surfaces had been coated with BG, the BG coating presumably was incomplete, especially the interior of the TCP ceramics possibly could not be coated with BG). Due to the continuous release of $[Ca^{2+}]$, the oversaturated $[Ca^{2+}]$ would react with $[H_xPO_4{}^{y-}]$ to form HA phasic minerals and release $[H^+]$ (chemical reaction formula (2)).[18] At the same time, $[Ca^{2+}]$ would bond with the sulfate groups of GS to form amorphous G-CaSO$_4$ (see the FTIR spectra, Fig. 2d(III)), chemical reaction formula (3)). The formed G-CaSO$_4$ would integrate with the HA phasic minerals to form the GS-containing HA nanocomposites (chemical reaction formula (4), Fig. 2a shows that a significant amount of GS remained in the ceramics after 160 h GS release). The above chemical reactions surely affected the microenvironment of the GS-loaded BG-TCP ceramics.

3.3. *In vitro* biological properties of the drug-loaded bioceramics

Although the biological properties of TCP and BG have been fully studied,[5,6,37] it has not been well understood how the microenvironment established by the drug-loaded bioceramics mediates the biological behaviours of MSCs. Herein, BM-MSCs were employed to assess the *in vitro* biological properties of the GS-loaded BG-TCP ceramics. At the same time, the TCP/BG-TCP ceramics were investigated as a control. BM-MSCs were used because they were osteogenic cell lines and the *in vitro* biological behaviours of BM-MSCs mediated by bioceramics can reflect *in vivo* bone regeneration events. To better understand the biological functions of ceramics *in vivo*, a surface mineralization experiment was performed by soaking bioceramics into SBF for 36 h before cell culture (when implanted into the body, bioceramics surely contact body liquid at first and likely react with the body liquid to grow the apatite nanoplate layers on the ceramic surfaces, and thus the cells *in vivo* in fact interact with the apatite nanoplate layers). SEM images show that the apatite nanoplate layer formed on the BG-TCP and GS/ BG-TCP ceramic surfaces, but not on the TCP ceramic surface (Fig. S4, ESI†).

At first, the survival and proliferation of MSCs on different ceramic surfaces were tested. The dead–live staining (Fig. 3a(I and II)) shows that only a few dead cells (red cells) were shown on day 1 on all ceramic surfaces and then there were hardly dead cells on all ceramic surfaces during the subsequent cell
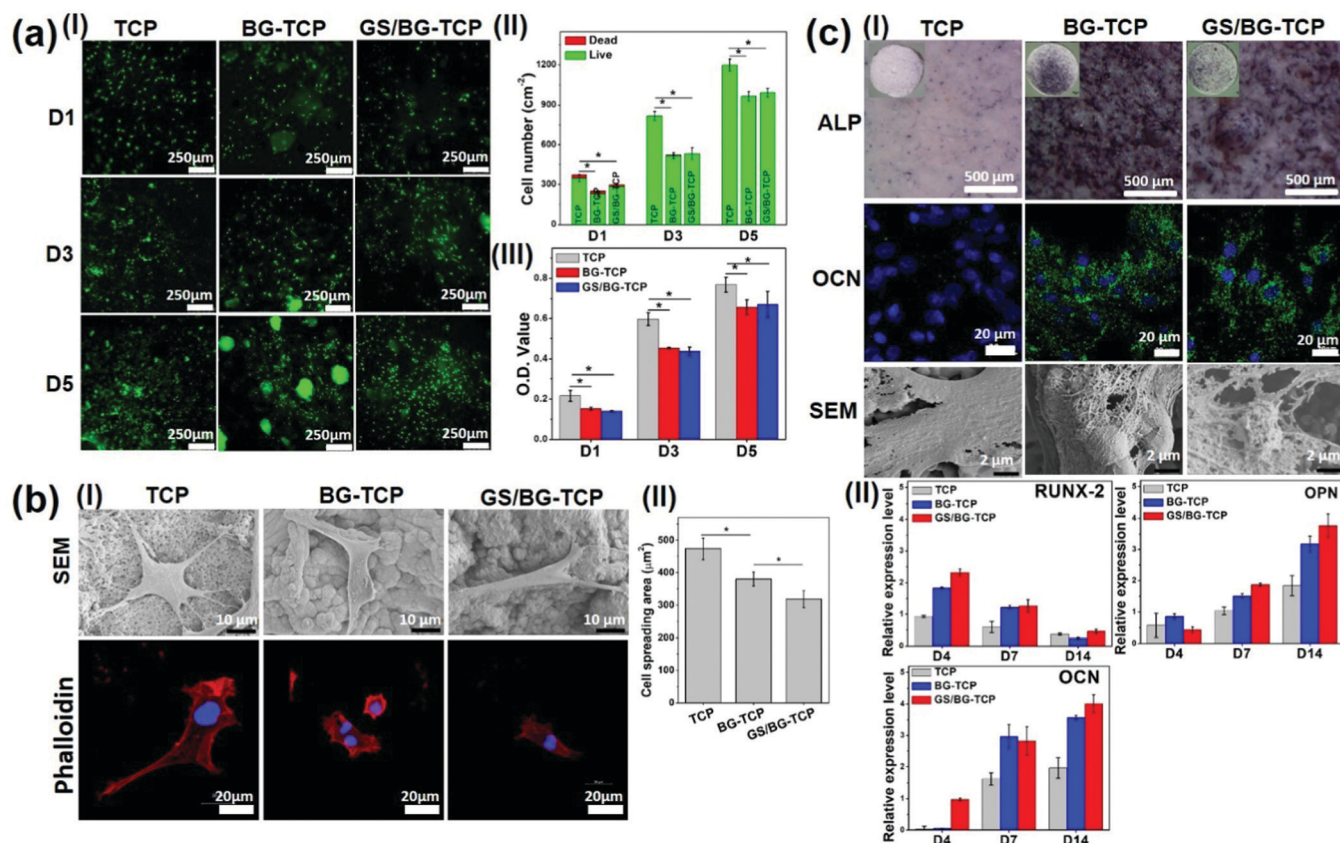
Fig. 3 *In vitro* biological behaviours of the BM-MSCs mediated by the porous ceramics. (a) Survival and proliferation of MSCs: (I and II) a dead−live staining (*n* = 3), (III) a quantitative CCK8 analysis (*n* = 3). (b) Cell adhesion and spreading: (I) SEM and phalloidin staining of BM-MSCs, and (II) the spreading area of cells on different ceramic surfaces (*n* = 7). (c) Osteogenic commitment of BM-MSCs. (I) ALP (day 4), OCN (day 14) and mineral nodule expression (day 14), and (II) RT-PCR analysis of the bone-relative gene expression (*n* = 3).

culture. However, the number of cells on the TCP ceramic surface appears to be significantly higher than that on the BG-TCP and GS/BG-TCP ceramic surfaces. A quantitative CCK8 analysis further confirmed such a result, as can be seen from Fig. 3a(III). The cells cultured on the TCP ceramics indicated a significantly higher O.D. value than those on the BG-TCP/GS/BG-TCP ceramics. Still, the proliferation tendency of cells on all ceramic surfaces was similar. The above results showed that the introduction of GS into ceramics did not cause cytotoxicity. The low survival of cells on the mineralized surfaces at the initial stage presumably resulted from a relatively high Ca^{2+} concentration released from the BG-containing ceramics (see Fig. 2c), which weakened the activity of integrins (a kind of adhesive protein),[38] and thus affected the adhesion of some cells on the mineralized surfaces during cell seeding.

Secondly, the adhesion behaviours of the MSCs cultured on the ceramic surfaces were analysed. SEM images (Fig. 3b(I)) show that the cells could well adhere and spread on the surfaces of all samples. Still, the spreading degree of the cells on different surfaces was different from each other (see Fig. 3b(I and II)). On the TCP surface, the cells expressed the strongest adhesion tension, and abundant filopodia and stress fibres were expressed. In contrast, the cells on the apatite nanoplate layer surfaces (BG-TCP and GS/BG-TCP) assembled

few filopodia and stress fibres, and thus resulted in a small spreading area in comparison with those on the TCP surface. Furthermore, Fig. 3b(II) shows that the existence of GS further affected the spread of cells.

Good adhesion of the cells on the TCP surface arose from the Ca-/P-sites on the TCP surface, which could interact non-specifically with the cell membrane proteins.[39,40] The high adhesion tension further triggered the cells to assemble the filopodia and stress fibers.[41] The decrease of the cytoskeleton tension in the cells mediated by the BG-TCP and GS/BG-TCP surfaces presumably could be attributed to the aligned nanoplates, which reduced the contact area of the cells (see Fig. 3b). In addition, the release of Ca^{2+} from the BG-containing ceramics (see Fig. 2c) would also possibly affect the activity of the integrins distributed on the cell membranes (it has well been demonstrated that integrins were Ca^{2+}-sensitive and high $[Ca^{2+}]_o$ could inhibit the activity of integrins),[38,42] and thus weaken the assembly of the cytoskeleton proteins.[38,42,43] As regards a further decrease of the cytoskeleton tension in the GS-mediated cells, a possible explanation is that the released GS would interact with membrane proteins (GS has abundant amide groups), and therefore interfering with the adhesion of the cells on the mineralized surfaces.[44]

Finally, the osteogenic commitment of MSCs mediated by the ceramics was assessed, and the corresponding results are

shown in Fig. 3c(I and II). ALP (an early bone-relative protein),[45] OCN (the mineral-relative proteins and can only be expressed by osteoblasts),[46] and mineral nodes all were secreted by the cells cultured on the mineralized BG-TCP and GS/BG-TCP surfaces, but not by those adhered on the TCP surface. Also, the quantitative (q-RT) PCR results show that in the cells cultured with the surface-mineralized ceramics, some important osteoblast-related genes, including RUNX-2, OPN and OCN, were activated in the correct order to permit differentiation, but the expression of these genes was weak in the cells cultured with the TCP ceramics. Furthermore, Fig. 3c(I and II) shows that the existence of GS did not affect the osteogenic commitment of MSCs.

Now, different signalling cues have been demonstrated to be able to mediate the osteogenic commitment of MSCs, including physical (e.g., surface stiffness[47] and special topographies[48]), chemical (e.g., $[Ca^{2+}]_o$[49,50] and $[H_xPO_4^{y-}]_o$[51]) and biological (a variety of growth factors, e.g., BMP-2/7[52,53]) factors. In our samples, the cues that could mediate the osteogenic commitment of MSCs mainly came from the physical (the surface stiffness and the grain-/nanoplate-constructed topography) and chemical (the Ca^{2+} release) factors. The physical cues can mediate the osteogenic differentiation of MSCs because the physical cues can mediate MSCs to generate a strong traction force to trigger the contraction-driving Rho A kinase (ROCK), which is central to the derivation of the high tensional state required for the osteogenic differentiation through activation of Rho A-initiating actin/myosin cytoskeletal contraction.[54] In our example, no osteogenic differentiation of MSCs that adhered on the TCP surfaces suggested that the traction force mediated by the TCP surface was not strong enough to activate ROCK. Also, ROCK in the cells adhered on the mineralized surfaces could not be activated because the mineralized surfaces mediated MSCs to form a smaller traction force. Therefore, the osteogenic differentiation of MSCs on the mineralized surfaces surely arose from the release of Ca^{2+} (see Fig. 2c). Maeno and our work well demonstrated that high concentration $[Ca^{2+}]_o$ could regulate the osteogenic differentiation of MSCs.[18,55] In addition, our results showed that the weak acidic microenvironment did not mediate the osteogenic commitment of MSCs (the TCP ceramics could cause a weak acidic environment, see Fig. 2b).

3.4. Antibacterial activity of the drug-loaded ceramics

To understand the antibacterial activity of the GS-loaded porous ceramics, Gram-positive bacteria S. aureus and Gram-negative bacteria E. coli were used here because most bone infections are caused by these bacteria.[56] At the same time, the TCP and BG-TCP porous ceramics were also assessed as a control. To determine the antibacterial activity of the ceramics, a sample transferring method was created in this work, i.e., a porous ceramic was incubated for 24 h in turn in fresh bacterial suspensions/disks.

At first, a quantitative analysis of the antibacterial activity was performed using the bacterial suspension assay.[57,58] Fig. 4(a) shows that the GS-loaded ceramics had very strong

antibacterial activity. After the ceramics had been incubated in 4 fresh bacterial suspensions, their antibacterial rate was still kept at 100% against two kinds of bacteria. Only after the fifth incubation, the antibacterial ability of the GS-loaded ceramics began to decrease. Such a result suggested that GS could be released under control and was well in accordance with the release profiles of GS (Fig. 2a). In contrast, the TCP and BG-TCP ceramics hardly presented the antibacterial activity in the S. aureus/E. coli suspensions.

A disk diffusion method was further performed to assess the antibacterial activity of the as-prepared ceramics (i.e., the inhibitory effect was tested on the basis of the clear zone surrounding the circular-shaped sample).[57,58] Fig. 4(b) shows that after 24 h incubation in the S. aureus/E. coli colony, a huge inhibition zone surrounding the GS-loaded ceramic (3.6 mm in the S. aureus colony, 3.7 mm in the E. coli colony) was formed. In contrast, in the TCP/BG-TCP ceramics, no inhibition zone was formed in the S. aureus/E. coli colony. Furthermore, the GS-loaded ceramic was transferred continuously to the disks with a fresh S. aureus/E. coli colony, and Fig. 4(c) shows that the inhibition zone reduced gradually, and during the sixth transfer of the GS-loaded ceramic, no inhibition zone was present around the ceramic. The disk diffusion method further confirmed that the release of the GS loaded in ceramics could be controlled.

3.5. In situ bone regeneration mediated by the drug-loaded ceramics

To assess the endogenous regenerative procedure of the bones mediated by the GS-loaded ceramics, circular bone defects ($\varnothing$: 5 mm) were created in the rabbit femurs (see Fig. S1, ESI†), and at the same time, the femoral marrow cavities of the rabbits were used as the ceramic implanting sites. Correspondingly, cylindrical ceramics were prepared ($\varnothing$: 5 mm, high: 5 mm). The femoral marrow cavity was selected to assess the osteogenic activity of implants because the femoral marrow cavity has abundant MSCs, which are the same in the cell lineage as bone cells and are important osteogenic cells for bone growth/remodelling, and at the same time, the femoral marrow cavity shares the microenvironment with bone tissue.[18]

Fig. 5(a) shows the histological sections of three kinds of ceramics that have implanted into the femoral marrow cavity for 6 weeks. The magnified images show that in the porosity of all ceramics a little new bone tissue formed, and some newly grown bone embedded into the micropores distributed on the ceramic substrates. The above results demonstrated that the BM-MSCs could migrate into ceramics and differentiate into bone tissue (it should be noted that in the TCP ceramics, new bone tissue could form in vivo but not in vitro (see Fig. 3c). Such a distinct result suggested that the in vitro MSC culture time was not long enough, or unknown cues existed in vivo, which could mediate the osteogenic differentiation of MSCs, e.g., myeloid cells or OsteoMac could induce the differentiation of BM-MSCs).[59] Still, the quantified bone mass (Fig. 5a) shows that the newly formed bone mass in the GS-loaded ceramics was significantly higher than that in the TCP ceramics, but was significantly lower than that in the GS-TCP ceramics. A possible
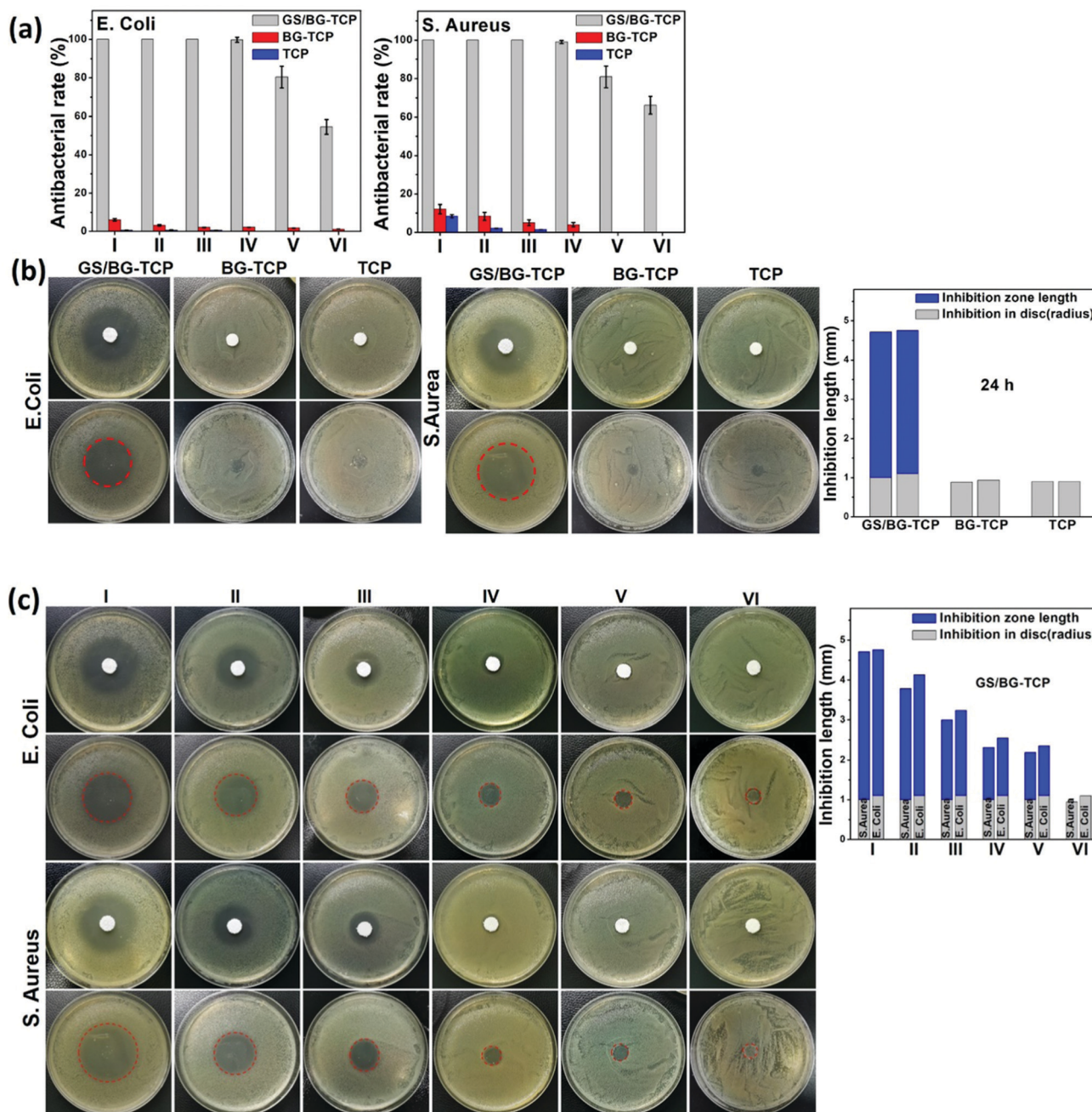
Fig. 4 *In vitro* antibacterial activity of the as-prepared porous ceramics. (a) Quantitative bacterial suspension assay (the individual ceramics were incubated in turn for 24 h in the 6 fresh bacterial suspensions. I–VI indicate the number of times the ceramics were incubated in the fresh bacterial suspension) (*n* = 3); (b) disk diffusion method to assess three kinds of ceramics (incubated for 24 h) (top disks: in order to observe the inhibition zone length, the incubated ceramics remained in the bacterial disks. Bottom disks: in order to observe the inhibition in ceramics, the incubated ceramics were removed); and (c) the disk diffusion method to assess the GS-loaded BG-TCP ceramics (the individual ceramics were incubated in turn for 24 h in the 6 fresh bacterial disks. I–VI indicate the number of times the ceramics were incubated in the fresh bacterial disk) (top disks: to observe the inhibition zone length, the incubated ceramics remained in the bacterial disks. Bottom disks: to observe the inhibition in ceramics, the incubated ceramics were removed).

explanation is that the difference of the released [Ca^{2+}] among three kinds of ceramics (see Fig. 2c) resulted in the ceramics with different ability to recruit MSCs into the ceramic pores.[35,60] Furthermore, our results, *i.e.*, the grown bone embedded into the substrate micropores, also suggested that the existence of micropores could promote bone regeneration.

In the sites of bone defects, Fig. 5(b) shows that new bone formed in all defects implanted by different ceramics (6 weeks). The photographs show that the ceramics were embedded well in the newly grown bone tissue, and new bone did not grow in the section of the ceramics that exceeded the bone surfaces. The histological sections show that in all samples new bone
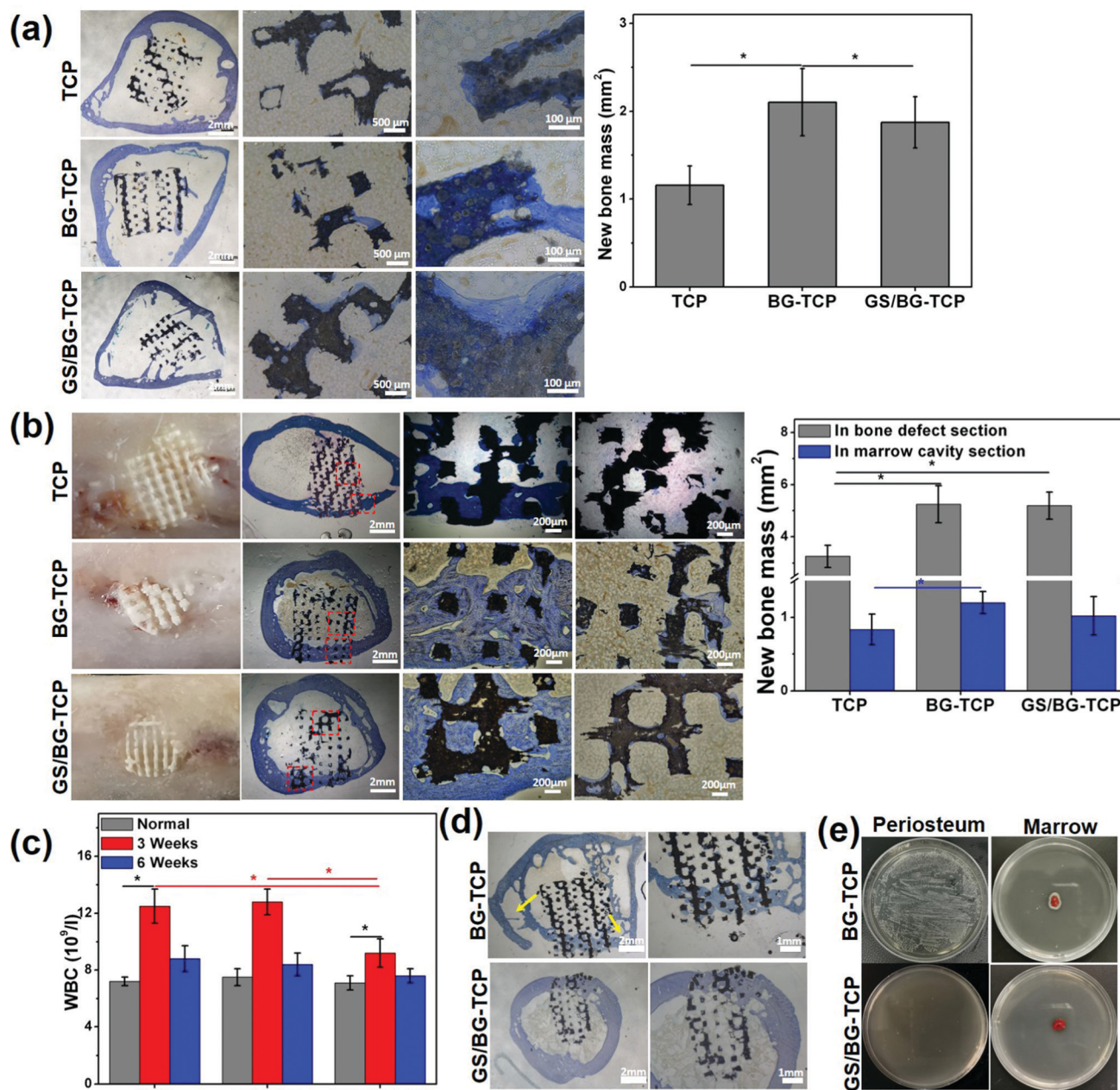
Fig. 5 The porous ceramic-mediated *in situ* regeneration of bone. (a) The TB-stained histological sections of the porous ceramics implanted into the femoral marrow cavities for 6 weeks (*n* = 3). (b) The TB-stained histological sections of the ceramics implanted into the femoral defects (5 mm) for 6 weeks (*n* = 3). (c) WBC of the rabbits in the normal and ceramic-implanted (3/6 weeks) state (*n* =3). (d) The ceramic-mediated *in situ* regeneration of bone in the *S. aureus*-infected bone defects (6 weeks) (the yellow arrows indicate the formation of cavitary defects). (e) The marrows harvested from the 6 week-ceramic implanted femurs were incubated for 24 h in the solid medium.

tissue grew well in the section of the ceramic embedded in the bone defect, but in the section of ceramics embedded in the marrow only a little bit of newly grown bone tissue adhered on the porous surfaces of the ceramics, and a clear bone-marrow interface was present in all ceramics. The quantitative bone mass shows that in the section of the ceramics distributed in bone defects, the bone mass grown in the GS-loaded ceramics was similar to that in the BG-TCP ceramics, but was significantly higher than that in the TCP ceramics. In the section of

the ceramics in the marrow, the bone mass grown in three kinds of ceramics was similar in ratio to that grown in the whole ceramics implanted in marrow cavities (Fig. 5a). The above results further demonstrated that it was the released Ca^{2+} that promoted the *in situ* regeneration of bone.

Furthermore, the WBC number of the ceramic-implanted rabbits was measured. The purpose of measuring the WBC number is that it has been well acknowledged that the normal inflammatory response played important roles in mediating the

endogenous regenerative procedure of tissues (normal tissue inflammation can recruit and activate a variety of cells, *e.g.*, immunocytes, endothelial cells, stem cells, *etc.*, to orchestrate tissue regeneration).[61] The change in the WBC number can reflect the inflammatory response of rabbits to the implanted ceramics. Fig. 5c shows the WBC value of normal and post-operative (3/6 weeks) rabbits. In comparison with the normal WBC value of rabbits, the WBC number increased significantly in all rabbits implanted with porous ceramics for 3 weeks. Still, the WBC value in the rabbits implanted with the GS-loaded ceramics expressed the lowest WBC number. Such a result showed that the implanting sites with the high concentration of GS could suppress the inflammatory response. After 6 weeks, Fig. 5c shows that the WBC number of all rabbits almost returned to the normal value. The above results demonstrated that more bone mass grown from the BG-containing ceramics did not arise from the tissue inflammation.

Taken together, our *in vivo* implanting experiments showed that all porous ceramics could mediate the endogenous regeneration of bone. In particular, in the bone defect sites, a clear bone-marrow interface within ceramics could form due to the as-prepared ceramics with regular porosity (our previous work has demonstrated that the ceramics with irregular porosity inhibited the formation of the bone-marrow interface).[18] Still, our experiments showed that the BG-containing porous ceramics promoted the body to regenerate more new bone. Such a difference was attributable to the dynamic microenvironment constructed by the BG-containing ceramics, in which the apatite nanoplate layer could grow on the ceramic surfaces. Previously, Bohner *et al.* and our group demonstrated the growth of an apatite nanoplate layer acting as an inorganic mineral ion adjuster in the microenvironment, and the change in the Ca^{2+} concentration has made a significant contribution to boosting the endogenous regeneration of bone.[6] In addition, our experiments showed that the weak acidic microenvironment did not boost bone growth. A possible explanation is that the acidic degree did not arrive at the critical value to trigger the extra inflammation of bone (a high WBC number expressed in all rabbits within 3 weeks should be attributed to the surgical operation and the implanted ceramics).[62] Also, our experiments also showed that the relatively high concentration of GS in the microenvironment (the highest release concentration of GS was <0.15 mg ml^{-1}) did not affect the endogenous regeneration of bone. Such a result is attributable to two factors: (i) GS was cytocompatibility (Fig. 3a), and (ii) GS in the microenvironment did not affect in essence the growth of the apatite nanoplate layer (in fact GS promoted the growth of the apatite nanoplate layer, see Fig. 2d).

Finally, the *in vivo* antibacterial activity of the as-prepared ceramics was checked by creating the *S. aureus*-infected bone defects as the implanting sites (see Fig. S3, ESI†). After the infected bone defects were washed, the BG-TCP ceramics and the GS/BG-TCP ceramics were implanted respectively in the bone defects for 6 weeks. The histological sections (Fig. 5d) show that new bone could grow in both ceramics. Nevertheless, in the BG-TCP ceramic treated bone defect, osteolysis seems to

have occurred in the femur (the arrows indicated the formation of cavitary defects). This suggested that some *S. aureus* still resided in the bone marrow because the existence of bacteria in the body would cause the inflammation response and thus macrophages/osteoclasts were recruited or stimulated to absorb bone due to the strong stimulatory effect by bacterial toxins.[58,63] To demonstrate this speculation, the periostea and marrows were harvested from the ceramic implanted femurs. Fig. 5(e) shows that some *S. aureus* indeed resided in the periosteum and marrow of the BG-TCP ceramic implanted femur. In contrast, in the GS-loaded ceramic-treated specimens, Fig. 5(e) shows that no bacteria were indicated. The above results demonstrated that our GS-loaded ceramics could prevent the bacterial infection from recurring.

Taken together, our *in vivo* experiments well demonstrated that the GS-loaded BG-TCP ceramics not only could mediate the *in situ* regeneration of bone, but also possessed high antibacterial activity against *S. aureus*. In particular, because the used biomaterials (BG and TCP) and drugs (GS) all have been widely applied in clinical practice, our samples have the potential to be exploited in commercial products.

4. Conclusions

BG-coated hierarchical porous TCP bioceramics were successfully prepared by combining 3D printing, gelcasting, and sol–gel coating methods. Abundant pores distributed hierarchically in ceramics endowed the ceramics with multiple biological functions. The macropores with regular porous structures allowed the growth of new bone only in the bone defect section and the formation of a clear bone-marrow interface. The nanopores endowed the ceramics with the drug delivery ability. More importantly, the coating of BG on the TCP ceramic surfaces constructed a dynamic microenvironment which could boost the endogenous regeneration of bone. The existence of a relatively high concentration of antibacterial drug GS (<0.15 mg ml^{-1}) in the microenvironment did not affect the endogenous regeneration of bone because the released GS in the microenvironment did not affect in essence the growth of an apatite nanoplate layer. Our experiments further demonstrated that the GS-loaded ceramics could prevent the bacterium-ever infected bone defects from recurring. Because the used ceramic materials, TCP and BG, have used widely in clinical practice, our porous ceramics have the potential for treating infected bone defects.

Conflicts of interest

There are no conflicts to declare.

Acknowledgements

Notes and references

1 G. L. Koons, M. Diba and A. G. Mikos, *Nat. Rev. Mater.*, 2020, **5**, 584–603.

2 A. K. Gaharwar, I. Singh and A. Khademhosseini, *Nat. Rev. Mater.*, 2020, **5**, 686–705.

3 K. L. Christman, *Science*, 2019, **363**, 340–341.

4 Y. Zhou, C. Wu and J. Chang, *Mater. Today*, 2019, **24**, 41–56.

5 Y. Hong, H. Fan, B. Li, B. Guo, M. Liu and X. Zhang, *Mater. Sci. Eng. R*, 2010, **70**, 225–242.

6 M. Bohner and R. J. Miron, *Mater. Today*, 2019, **22**, 132–141.

7 D. Zhang, M. Hupa and L. Hupa, *Acta Biomater.*, 2008, **4**, 1498–1505.

8 Y. Shen, W. Liu, C. Wen, H. Pan, T. Wang, B. W. Darvell, W. W. Lu and W. Huang, *J. Mater. Chem.*, 2012, **22**, 8662–8670.

9 Y. Maazouz, I. Rentsch, B. Lu, B. L. G. Santoni, N. Doebelin and M. Bohner, *Acta Biomater.*, 2020, **102**, 440–457.

10 U. Ripamonti, R. M. Klar, L. F. Renton and C. Ferretti, *Biomaterials*, 2010, **31**, 6400–6410.

11 P. Habibovic, H. Yuan, C. M. van der Valk, G. Meijer, C. A. van Blitterswijk and K. de Groot, *Biomaterials*, 2005, **26**, 3565–3575.

12 S. Fujibayashi, M. Neo, H. M. Kim, T. Kokubo and T. Nakamura, *Biomaterials*, 2004, **25**, 443–450.

13 D. Barbieri, A. J. S. Renard, J. D. de Bruijn and H. Yuan, *Eur. Cells Mater.*, 2010, **19**, 252–261.

14 Y. Chen, Z. Sun, Y. Li and Y. Hong, *J. Mater. Chem. B*, 2017, **5**, 807–816.

15 C. Zhou, Y. Jiang, Z. Sun, Y. Li, B. Guo and Y. Hong, *J. Mater. Chem. B*, 2018, **6**, 5621–5632.

16 Y. Chen, Z. Sun, Y. Li and Y. Hong, *J. Mater. Chem. B*, 2017, **5**, 807–816.

17 M. J. Dalby, N. Gadegaard and R. O. C. Oreffo, *Nat. Mater.*, 2014, **13**, 558–569.

18 W. He, Z. Wu, Y. Wu, Z. Zhong and Y. Hong, *ACS Appl. Mater. Interfaces*, 2021, **13**, 31527–31541.

19 S. K. Nandi, S. Bandyopadhyay, P. Das, I. Samanta, P. Mukherjee, S. Roy and B. Kundu, *Biotechnol. Adv.*, 2016, **34**, 1305–1317.

20 N. H. Besheli, F. Mottaghitalab, M. Eslami, M. Gholami, S. C. Kundu, D. L. Kaplan and M. Farokhi, *ACS Appl. Mater. Interfaces*, 2017, **9**, 5128–5138.

21 P. Wei, W. Jing, Z. Yuan, Y. Huang, B. Guan, W. Zhang, X. Zhang, J. Mao, Q. Cai, D. Chen and X. Yang, *ACS Appl. Mater. Interfaces*, 2019, **11**, 30596–30609.

22 I. Qayoom, A. K. Teotia, A. Panjla, S. Verma and A. Kumar, *ACS Infect. Dis.*, 2020, **6**, 2938–2949.

23 J. Geurts, J. J. Chris Arts and G. H. Walenkamp, *Injury*, 2011, **42**, S82–S86.

24 Y. Deng, X. Shi, Y. Chen, W. Yang, Y. Ma, X.-L. Shi, P. Song, M. S. Dargusch and Z.-G. Chen, *Ind. Eng. Chem. Res.*, 2020, **59**, 12123–12135.

25 Y. Deng, X. Gao, X.-L. Shi, S. Lu, W. Yang, C. Duan and Z.-G. Chen, *Chem. Mater.*, 2020, **32**, 2180–2193.

26 S. Wang, C. Duan, W. Yang, X. Gao, J. Shi, J. Kang, Y. Deng, X.-L. Shi and Z.-G. Chen, *Nanoscale*, 2020, **12**, 11936–11946.

27 S. J. Hollister, *Nat. Mater.*, 2005, **4**, 518–524.

28 L. L. Hench, *J. Am. Ceram. Soc.*, 1998, **81**, 1705–1728.

29 W. Liu, T. Wang, X. Zhao, X. Dan, W. W. Lu and H. Pan, *Bioact. Mater.*, 2016, **1**, 151–159.

30 Y. Shen, W. Liu, K. Lin, H. Pan, B. W. Darvell, S. Peng, C. Wen, L. Deng, W. W. Lu and J. Chang, *Langmuir*, 2011, **27**, 2701–2708.

31 Y. Hong, H. Fan and X. Zhang, *J. Phys. Chem. B*, 2009, **113**, 5837–5842.

32 Y. Hong, X. Chen, X. Jing, H. Fan, B. Guo, Z. Gu and X. Zhang, *Adv. Mater.*, 2010, **22**, 754–758.

33 X. X. Yan, H. X. Deng, X. H. H. Huang, M. Lu, S. Qiao, D. Y. Zhao and C. Z. Yu, *J. Non-Crystalline Solids*, 2005, **351**, 3209–3217.

34 Y. Chen, Z. Sun, Y. Li and Y. Hong, *J. Mater. Chem. B*, 2017, **5**, 807–816.

35 I. T. Olszak, M. C. Poznansky, R. H. Evans, D. Olson, C. Kos, M. R. Pollak, E. M. Brown and D. T. Scadden, *J. Clin. Invest.*, 2000, **105**, 1299–1305.

36 C. Tan, Z. Sun, Y. Hong, Y. Li, X. Chen and X. Zhang, *J. Mater. Chem. B*, 2013, **1**, 3694–3704.

37 L. L. Hench, *J. Mater. Sci.: Mater. Med.*, 2015, **26**, 86.

38 K. Zhang and J. Chen, *Cell Adhes. Migr.*, 2012, **6**, 20–29.

39 K. Kandori, T. Kuroda, S. Togashi and E. Katayama, *J. Phys. Chem. B*, 2011, **115**, 653–659.

40 K. Kandori, K. Murata and T. Ishikawa, *Langmuir*, 2007, **23**, 2064–2070.

41 A. L. Berrier and K. M. Yamada, *J. Cell. Physiol.*, 2007, **213**, 565–573.

42 D. D. Hu, J. R. Hoyer and J. W. Smith, *J. Bio. Chem.*, 1995, **270**, 9917–9925.

43 M. Shimaoka, J. Takagi and T. A. Springer, *Annu. Rev. Biophys. Biomol. Struct.*, 2002, **31**, 485–516.

44 C. K. Miranti and J. S. Brugge, *Nat. Cell Biol.*, 2002, **4**, E83–E90.

45 N. D. Escudero and P. M. Mandalunis, *Bone*, 2007, **40**, S7.

46 P. Ducy, C. Desbois, B. Boyce, G. Pinero, B. Story, C. Dunstan, E. Smith, J. Bonadio, S. Goldstein, C. Gundberg, A. Bradley and G. Karsenty, *Nature*, 1996, **382**, 448–452.

47 A. J. Engler, S. Sen, H. L. Sweeney and D. E. Discher, *Cell*, 2006, **126**, 677–689.

48 M. J. Dalby, N. Gadegaard, R. Tare, A. Andar, M. O. Riehle, P. Herzyk, C. D. W. Wilkinson and R. O. C. Oreffo, *Nat. Mater.*, 2007, **6**, 997–1003.

49 T. Sugimoto, M. Kanatani, J. Kano, H. Kaji, T. Tsukamoto, T. Yamaguchi, M. Fukase and K. Chihara, *J. Bone Miner. Res.*, 1993, **8**, 1445–1452.

50 E. M. Brown and R. J. Macleod, *Physiol. Rev.*, 2001, **81**, 239–297.

51 Y.-R. V. Shih, Y. Hwang, A. Phadke, H. Kang, N. S. Hwang, E. J. Caro, S. Nguyen, M. Siu, E. A. Theodorakis, N. C. Gianneschi, K. S. Vecchio, S. Chien, O. K. Lee and S. Varghese, *Proc. Natl. Acad. Sci. U. S. A.*, 2014, **111**, 990–995.

52 U. Ripamonti and J.-C. Petit, *Cytokine Growth Factor Rev.*, 2009, **20**, 489–499.

53 U. Ripamonti, *Biomaterials*, 2006, **27**, 807–822.

54 R. McBeath, D. M. Pirone, C. M. Nelson, K. Bhadriraju and C. S. Chen, *Dev. Cell*, 2004, **6**, 483–495.

55 S. Maeno, Y. Niki, H. Matsumoto, H. Morioka, T. Yatabe, A. Funayama, Y. Toyama, T. Taguchi and J. Tanaka, *Biomaterials*, 2005, **26**, 4847–4855.

56 G. Walter, M. Kemmerer, C. Kappler and R. Hoffmann, *Dtsch. Arztebl. Int.*, 2012, **109**, 257–264.

57 Z. Wu and Y. Hong, *ACS Appl. Mater. Interfaces*, 2019, **11**, 33734–33747.

58 W. He, Z. Wu, Y. Wu, Y. Cai, Z. Cui, B. Yu and Y. Hong, *ACS Appl. Bio Mater.*, 2021, **4**, 6280–6293.

59 L. Batoon, S. M. Millard, L. J. Raggatt and A. R. Pettit, *Curr. Osteoporos. Rep.*, 2017, **15**, 385–395.

60 T. Yamaguchi, I. Olozak, N. Chattopadhyay, R. R. Butters, O. Kifor, D. T. Scadden and E. M. Brown, *Biochem. Biophys. Res. Commun.*, 1998, **246**, 501–506.

61 T. A. Wynn and K. M. Vannella, *Immunity*, 2016, **44**, 450–462.

62 J. M. Anderson, A. Rodriguez and D. T. Chang, *Semin. Immunol.*, 2008, **20**, 86–100.

63 J. Lorenzo, M. C. Horowitz, Y. Choi, H. Takayanagi and G. Schett, *Osteoimmunology: Interactions of the Immune and Skeletal Systems*, Academic Press, 2nd edn, 2015.